25th AIAA Aerodynamic Measurement Technology and Ground Testing Conference
5 - 8 June 2006, San Francisco, California

AIAA 2006-2969

Molecular Rayleigh Scattering Diagnostic for Dynamic Temperature, Velocity, and Density Measurements

Amy F. Mielke*
NASA Glenn Research Center, Cleveland, OH, 44135

Kristie A. Elam†
Jacobs Sverdrup, Cleveland, OH, 44135

and

Chih-Jen Sung‡
Case Western Reserve University, Cleveland, OH, 44106

A molecular Rayleigh scattering technique is developed to measure dynamic gas temperature, velocity, and density in unseeded turbulent flows at sampling rates up to 16 kHz. A high power CW laser beam is focused at a point in an air jet plume and Rayleigh scattered light is collected and spectrally resolved. The spectrum of the light, which contains information about the temperature and velocity of the flow, is analyzed using a Fabry-Perot interferometer. The circular interference fringe pattern is divided into four concentric regions and sampled at 1 and 16 kHz using photon counting electronics. Monitoring the relative change in intensity within each region allows for measurement of gas temperature and velocity. Independently monitoring the total scattered light intensity provides a measure of gas density. A low speed heated jet is used to validate the measurement of temperature fluctuations and an acoustically excited nozzle flow is studied to validate velocity fluctuation measurements. Power spectral density calculations of the property fluctuations, as well as mean and fluctuating quantities are presented. Temperature fluctuation results are compared with constant current anemometry measurements and velocity fluctuation results are compared with constant temperature anemometry measurements at the same locations.

Nomenclature

a	=	most probable molecular speed (m s^{-1})
c	=	speed of light (= 2.998 x 10^8 m s^{-1})
d	=	Fabry-Perot mirror spacing (m)
$\mathbf{E}$	=	incident electric field vector (N C^{-1})
F	=	Fabry-Perot instrument function contrast
f	=	frequency of scattered light (s^{-1})
f_0	=	frequency of incident laser light (s^{-1})
f_C	=	collimating lens focal length (m)
f_L	=	fringe forming lens focal length (m)
f_s	=	sampling rate (s^{-1})
h	=	Planck's constant (= 6.626 x 10^{-34} N m s)
I_{FP}	=	Fabry-Perot instrument function
$\mathbf{K}$	=	interaction wave vector (m^{-1})
K	=	magnitude of $\mathbf{K}$ (m^{-1})
$\mathbf{k_0}$	=	incident light wave vector (m^{-1})

* Research Engineer, Optical Instrumentation and NDE Branch, Member AIAA
† Optics Technician
‡ Associate Professor, Department of Mechanical and Aerospace Engineering, Senior Member AIAA

$\mathbf{k_s}$ = scattered light wave vector (m^{-1})
L = length of sub-records in spectral calculations
L_x = probe volume length (m)
l_m = mean free path between molecular collisions (m)
m = molecular mass (kg)
N_e = effective finesse
N_q = photoelectron counts at q^{th} annular region
N_R = Rayleigh scattered photoelectrons collected into solid angle Ω
n = molecular number density (m^{-3})
P_0 = power of incident laser beam ($J\ s^{-1}$)
p = static pressure ($N\ m^{-2}$)
q = annular region number
r = radial position in image plane (m)
r_j = radial position in the jet measurement plane (m)
r_{max} = fiber face image radius (m)
r_q = inner radius of q^{th} annular region (m)
r_R = fringe radius associated with reference laser light (m)
S_R = Rayleigh scattering spectrum
T = static temperature (K)
$\mathbf{u}$ = velocity vector ($m\ s^{-1}$)
u_k = measured velocity component ($m\ s^{-1}$)
x_f = frequency shift non-dimensionalized by the frequency shift related to the local speed of sound
y = y-parameter
β = angle between $\mathbf{E}$ and $\mathbf{k_s}$ vectors (rad)
Γ = Fisher information matrix
Δr = width of annular region (m)
Δt = integration time (s)
ε = optical system efficiency
η = dynamic viscosity ($N\ s\ m^{-2}$)
θ = angle between light ray and optical axis (rad)
θ_R = angle between reference light ray and optical axis (rad)
κ = Boltzmann's constant (= $1.381 \times 10^{-23}\ J\ K^{-1}$)
Λ = wavelength corresponding to wave vector $\mathbf{K}$ (m)
λ = illumination wavelength (m)
μ = refractive index
ρ = gas density ($kg\ m^{-3}$)
$\frac{d\sigma}{d\Omega}$ = differential scattering cross-section ($m^2\ sr^{-1}$)
χ_s = scattering angle (rad)
ψ = phase change between successive reflections
Ω = solid angle (sr)

I. Introduction

There is currently no high frequency response, non-intrusive temperature measurement technique for use in turbulent flow studies. There are also no techniques that can provide non-intrusive dynamic measurement of gas temperature, velocity, and density simultaneously. Conventional intrusive measurement devices such as resistance wires, pressure probes, and thermocouples are usually limited in spatial and temporal response, disturb the flow under study, and can be damaged by high pressure or temperature. Therefore, a non-intrusive molecular Rayleigh scattering technique is developed to measure dynamic gas temperature, velocity, and density in unseeded turbulent flows at sampling rates up to 16 kHz.

Various optical techniques are available for temperature, molecular number density, and velocity measurements. Eckbreth[1] provides the details of several techniques, such as Coherent Anti-Stokes Raman Spectroscopy (CARS), Spontaneous Raman and Rayleigh scattering, and Laser-Induced Fluorescence (LIF), with an emphasis on their use in combustion applications. Other techniques that have been used for flow measurements in various environments

include Laser-Induced Thermal Acoustics (LITA)[2,3], also known as Transient Grating Spectroscopy (TGS)[4], Laser-Doppler Velocimetry (LDV)[5-8], filtered Rayleigh scattering[9], Particle Image Velocimetry (PIV)[10], and focusing schlieren deflectometry[11]. However, none of these techniques can provide high frequency response measurement of all three flow properties simultaneously.

The temporal response of most of the optical measurement techniques mentioned here is typically limited by the repetition rate of pulsed lasers, usually on the order of 10 Hz; however one can potentially take many snap shots (1-5 ns temporal resolution) to obtain turbulence measurements. Signal strength of the scattering process can also limit the temporal response. Rayleigh scattering has several advantages over other light scattering techniques. The Rayleigh scattering cross-section is three orders of magnitude greater than the Raman scattering cross-section, and Rayleigh scattering is generally much simpler and lower cost to implement than techniques that require multiple lasers and have other complicating factors.

Previous works using molecular Rayleigh scattering to make temperature, velocity, and number density measurements in harsh environments have been reported[12-15]. The current work is an extension of a previously developed technique using Rayleigh scattering to obtain dynamic density and velocity measurements in supersonic free jets[16,17] and dynamic density and temperature measurements in heated jets[18]. The current work describes enhancements to the technique previously reported in which dynamic temperature, velocity, and density measurements were made in a low speed heated jet up to a sampling rate of 10 kHz[19]. The Rayleigh scattering technique presented is unique in that it provides simultaneous temperature, velocity, and density fluctuation measurements. A high power CW laser beam is focused at a point in a jet plume and Rayleigh scattered light is collected and spectrally resolved. The spectrum of the light contains information about the temperature, velocity, and density of the flow. A planar mirror Fabry-Perot interferometer (FPI) is used to analyze the spectrum of the scattered light, and photomultiplier tubes (PMTs) record the fringe intensity pattern at high sampling rates enabling dynamic measurement of the gas flow properties. The enhancements of the technique over that previously reported[19] include the use of a laser with twice the output power, which enables sampling at higher rates, improvement of the image dissection system, and improvements in the data processing methods. Analysis of the various factors contributing to bias errors in the velocity estimates has led to a better understanding of how to improve the measurements. A low speed heated jet was used to verify the temperature fluctuation measurements with the enhanced system and an acoustically excited jet was used to validate the velocity fluctuation and frequency measurements.

The ability to obtain high frequency response measurement of multiple properties simultaneously is a valuable tool for compressible, turbulent flow research. These data are particularly useful to aeroacoustics researchers who are interested in correlating flow property fluctuations with far field acoustic fluctuations. Knowledge of velocity-temperature fluctuation correlations is also needed to improve computational fluid dynamic (CFD) models of compressible turbulent flows.

II. Theory

A. Rayleigh scattering and spectral analysis

Molecular Rayleigh scattering is the result of elastic light scattering from gas molecules. When light from a single frequency laser beam passes through a gas, the scattered light is shifted in frequency by the Doppler effect due to the thermal as well as the bulk motion of the molecules. The frequency spectrum of the scattered light contains information about the gas density, bulk velocity, and temperature. Figure 1 shows a Rayleigh scattering spectrum containing the narrow laser line and a typical Rayleigh spectral peak to illustrate how the flow property measurements are obtained from the spectral information. If the gas composition is fixed, the total intensity of the Rayleigh scattered light is directly proportional to the gas density. The frequency shift between the laser peak and the Rayleigh peak is proportional to the bulk flow velocity. The width of the spectrum is related to the gas temperature.

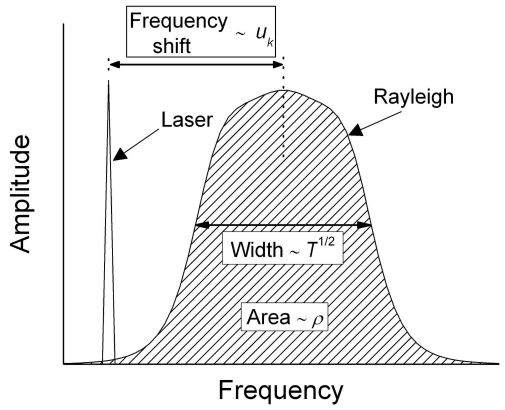

Figure 1. Rayleigh scattering spectrum.

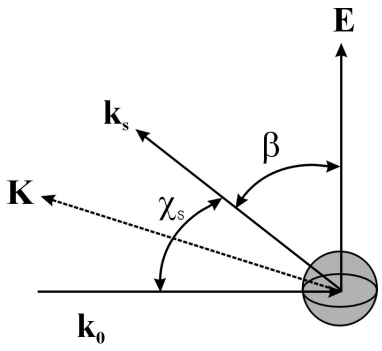

Figure 2. Light scattering from a moving particle.

The shape of the spectrum is dependent on gas pressure, temperature and the scattering angle[20]. A non-dimensional parameter *y*, which represents the ratio of the wavelength of the scattering grating $\left(\Lambda = \frac{\lambda}{2\sin\frac{\chi_s}{2}}\right)$ to the mean free path between molecular collisions $\left(l_m = \frac{n\kappa T}{a\eta}\right)$, is used to establish spectral shape regimes:

$$y = \frac{\Lambda}{2\pi\, l_m} = \frac{p}{\eta K a} \tag{1}$$

where

$$a = \sqrt{\frac{2\kappa T}{m}} \tag{2}$$

The interaction wave vector, which defines the direction of the velocity component being measured, is the bisector of the incident and scattered light wave vectors (Fig. 2). The interaction wave vector and its magnitude are given by:

$$\mathbf{K} = \mathbf{k_s} - \mathbf{k_0} \tag{3}$$

$$K = |\mathbf{K}| = \frac{4\pi}{\lambda}\left[\sin\frac{\chi_s}{2}\right] \tag{4}$$

The geometry of the optical arrangement in an experiment can be designed such that the desired component of the velocity is measured:

$$u_k = \frac{\mathbf{K}\cdot\mathbf{u}}{K} \tag{5}$$

Three spectral shape regimes are defined for typical 90° scattering[20-22]. For low density gases where $y << 1$, the Rayleigh spectrum is accurately modeled by a Gaussian function and the gas is said to be in the Knudsen or collisionless regime. For higher density gases where $y >> 1$, the Rayleigh spectrum broadens and eventually develops side-lobes known as Brillouin peaks. This is known as the hydrodynamic or continuum regime where molecular collisions are the dominant process. Finally, for $0.2 \le y \le 2$, as is the case in the present experiments, the gas is in a transition region between the collisionless and hydrodynamic regimes, and a kinetic theory model is required. The shape regimes are illustrated in Fig. 3, where the normalized frequency is defined as:

$$x_f = \frac{2\pi(f - f_0)}{Ka} \tag{6}$$

A kinetic theory model developed by G. Tenti[20,23] (TENTI S6) provides a description of Rayleigh-Brillouin scattering from molecular gases in all density regimes. This spectrum model was used to generate the information displayed in Figs. 1 and 3, and is incorporated in the model function used in least squares analysis of the experimental data.

The spectrum of the Rayleigh scattered light is analyzed using a planar mirror FPI (Fig. 4) operated in the static imaging mode[24]. The fringe intensity pattern is a function of both the Rayleigh spectrum and the Fabry-Perot instrument function. The Fabry-Perot instrument function is:

$$I_{FP}(x_f, r) = \frac{1}{1 + F \sin^2 \frac{\psi(x_f, r)}{2}} \tag{7}$$

where

$$F = \frac{1}{\sin^2\left(\frac{\pi}{2N_e}\right)} \tag{8}$$

$$\psi = \frac{4\pi\mu d}{\lambda}\left[\frac{\theta_R^2 - \theta^2}{2} + \frac{\lambda a}{c\Lambda} x_f\right] \tag{9}$$

$$\theta = r/f_L \tag{10}$$

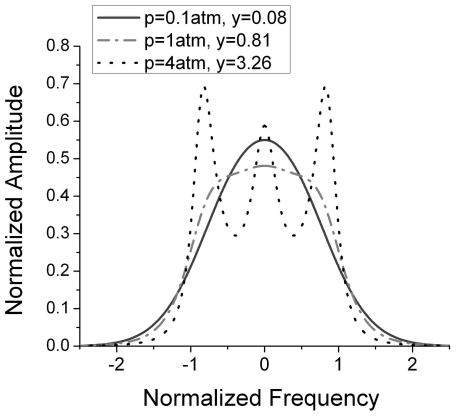

Figure 3. Rayleigh scattering spectrum for various *y*-parameters.

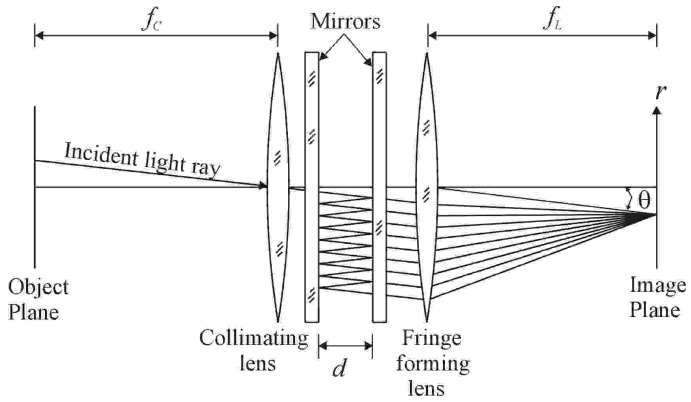

Figure 4. Fabry-Perot Interferometer.

In our experiment, Rayleigh scattered light from a defined probe volume is collected into a multimode optical fiber. The fiber directs the light to the FPI and a lens at the interferometer output focuses the interference fringe pattern at the image plane. The total expected number of Rayleigh photoelectron counts *without* the FPI in the optical path can be expressed as:

$$\langle N_R \rangle = \frac{\varepsilon P_0 n L_x \lambda \Omega \Delta t}{h c}\left(\frac{d\sigma}{d\Omega}\right)\sin^2\beta \tag{11}$$

where the overall system efficiency ε includes detector quantum efficiency and other losses. When the interferometer is placed in the light path, the model function for the amount of energy collected from the q^{th} annular

region of the interference pattern, which has been dissected into one circular and three annular regions, in terms of photoelectron counts, can be expressed as follows:

$$\left\langle N_q \right\rangle = \frac{\left\langle N_R \right\rangle}{\pi r_{\max}^2} \int_{r_q}^{r_q+\Delta r} \int_{-\infty}^{\infty} S_R(x_f)\, I_{FP}(x_f, r)\, dx_f\, dr \tag{12}$$

where the Rayleigh spectrum is evaluated using the TENTI S6 model.

B. Lower bound for measurement uncertainty

The lower bound on the uncertainty in temperature, velocity, and density measurements using Rayleigh scattering is set by the photon statistical (shot) noise. Estimates of the measurement uncertainty in the unknown parameters for this technique were obtained by Cramer-Rao lower bound analysis[25]. For a measurement that is a function of a set of unknown parameters, $\hat{\alpha}_i$, the variance of the estimates of the parameters is:

$$V(\hat{\alpha}_i) = \left\lfloor \Gamma^{-1} \right\rfloor_{ii} \tag{13}$$

where the Fisher information matrix for Poisson statistics is given by:

$$\Gamma_{i,j} = \sum_q \frac{1}{\left\langle N_q \right\rangle} \frac{\partial \left\langle N_q \right\rangle}{\partial \alpha_i} \frac{\partial \left\langle N_q \right\rangle}{\partial \alpha_j} \tag{14}$$

Using the model function developed for $\left\langle N_q \right\rangle$, the uncertainty or standard deviation $\sigma(\hat{\alpha}_i)$ in each unknown parameter may be determined by calculation and inversion of the Fisher information matrix.

If a Gaussian spectrum is assumed, the lower bounds for uncertainties in temperature T, velocity u_k, and density ρ for an ideal instrument are:

$$\begin{aligned} \frac{\sigma(T)}{T} &= \left(\frac{2}{\left\langle N_R \right\rangle} \right)^{1/2} \\ \frac{\sigma(u_k)}{a} &= \left(\frac{1}{2\left\langle N_R \right\rangle} \right)^{1/2} \\ \frac{\sigma(\rho)}{\rho} &= \left(\frac{1}{\left\langle N_R \right\rangle} \right)^{1/2} \end{aligned} \tag{15}$$

For air flow at T = 293 K, u_k = 100 m/s, and standard pressure, the lower bound uncertainty estimates for a sampling rate of 16 kHz, assuming an *ideal* instrument, are:

$$\frac{\sigma(T)}{T} = 1.4\,\% \qquad \sigma(u_k) = 4.2 \text{ m/s} \qquad \frac{\sigma(\rho)}{\rho} = 3.5\,\%$$

For any *real* instrument, these measurement uncertainties will be higher. The actual Cramer-Rao lower bound measurement uncertainties were calculated, given the Fabry-Perot interferometer, PMTs, and overall efficiency of the current system at the maximum sampling rate of 16 kHz. The TENTI S6 spectral model[20,23] was used to calculate the Rayleigh scattering spectrum in this analysis rather than using the simpler, less accurate Gaussian model used in the analysis above. Figure 5 shows the relative uncertainty in T over the range of velocities and temperatures covered in these experiments. Figure 6 gives the absolute uncertainty in u_k over the same range of velocities and temperatures. The measurement uncertainty increases as temperature increases. This is attributable to the lower gas

density at higher temperatures, resulting in fewer scattering molecules, and hence fewer scattered photons. Although the uncertainty in the parameters is rather high for instantaneous measurements, long data records allow for calculation of higher accuracy statistical quantities such as power spectra and mean square fluctuations. As sampling rate decreases, so will uncertainties, since the uncertainty is inversely related to the total number of photon counts, as shown in Eq. 15. Experimental data was acquired at sampling rates of 1 and 16 kHz. The lower sampling rate increased photon counts by a factor of 16, thereby improving uncertainty levels by a factor of $\sqrt{16}$ over the higher sampling rate.

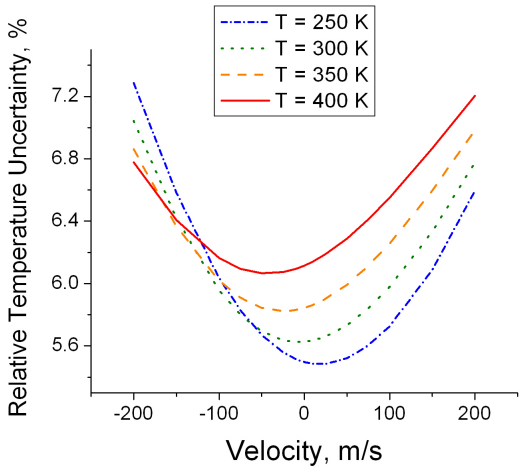

Figure 5. Relative uncertainty in temperature as a function of velocity and temperature.

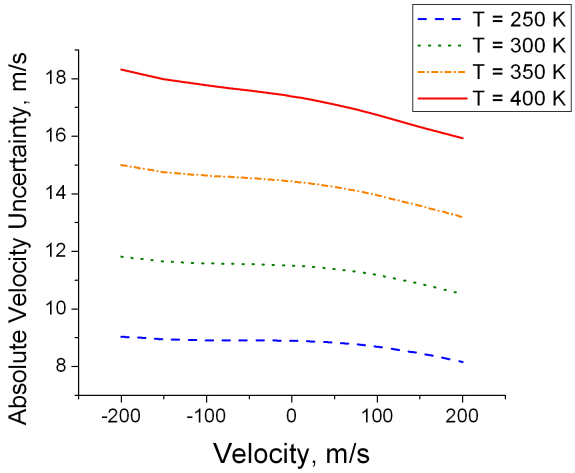

Figure 6. Absolute uncertainty in velocity as a function of velocity and temperature.

The Cramer-Rao lower bound analysis was used to design the controllable experiment parameters, such as magnification factor, reference fringe radius (r_R), and the radii of the fringe dissection mirrors. The parameters were varied in the model until the uncertainty levels in both T and u_k were minimized. A r_R value of 6.5 mm, image magnification of 33, and dissection mirror radii of 2.5 mm, 6 mm, 8 mm, and 12.5 mm were chosen for the experiments. The system is aligned such that the negative velocity component is measured. The velocity and temperature ranges of the experiments are -210 m/s – 0 m/s and 275 – 375 K.

III. Experiment

Two jet flow systems were used to evaluate the performance of the Rayleigh scattering flow diagnostic. A low speed electrically-heated jet was used to evaluate the ability to measure temperature fluctuations accurately by comparison with constant current anemometry (CCA) measurements. An acoustically-excited nozzle flow was used to validate velocity fluctuation and frequency measurements. The amplitude and frequency of the velocity fluctuations were verified by constant temperature anemometry (CTA) measurements. The details of the two experiments will be discussed in this section.

A. Optical Setup

Flow measurements were performed in an air stream issuing from a jet. Since the measurement technique relies on having particulate free gas flows, a series of filters were placed in line with the air plumbing to remove dust, oil and water from the air supply. Figure 7a shows the layout of the optics around the jet, which were used to collect Rayleigh scattered light from gas molecules in the flow. The jet shown in the diagram represents the acoustically-excited jet system. The jet was mounted such that the main flow direction was parallel to the table. A 10W, 532 nm wavelength, single-frequency, Nd:Vanadate CW laser provided incident light for the system. The laser beam was focused with a 250 mm focal length lens (L1) to a 70 μm $1/e^2$ diameter at the probe volume. The beam was oriented in the horizontal plane, at a 45° angle to the primary flow direction. Light was collected at a 90° scattering angle, collimated by a f/4 200 mm focal length lens (L2), and focused by a 100 mm focal length lens (L3) onto a 0.55 mm diameter multimode optical fiber. Since the pair of lenses provided 1:2 imaging, the length of the probe volume was 1.1 mm. The incident and scattering wave vectors were arranged such that the axial component of the jet velocity

was measured, as shown in Fig. 7a. The jet was mounted on vertical and horizontal translation stages so that the 1.1 mm probe volume could be positioned anywhere in the jet plume.

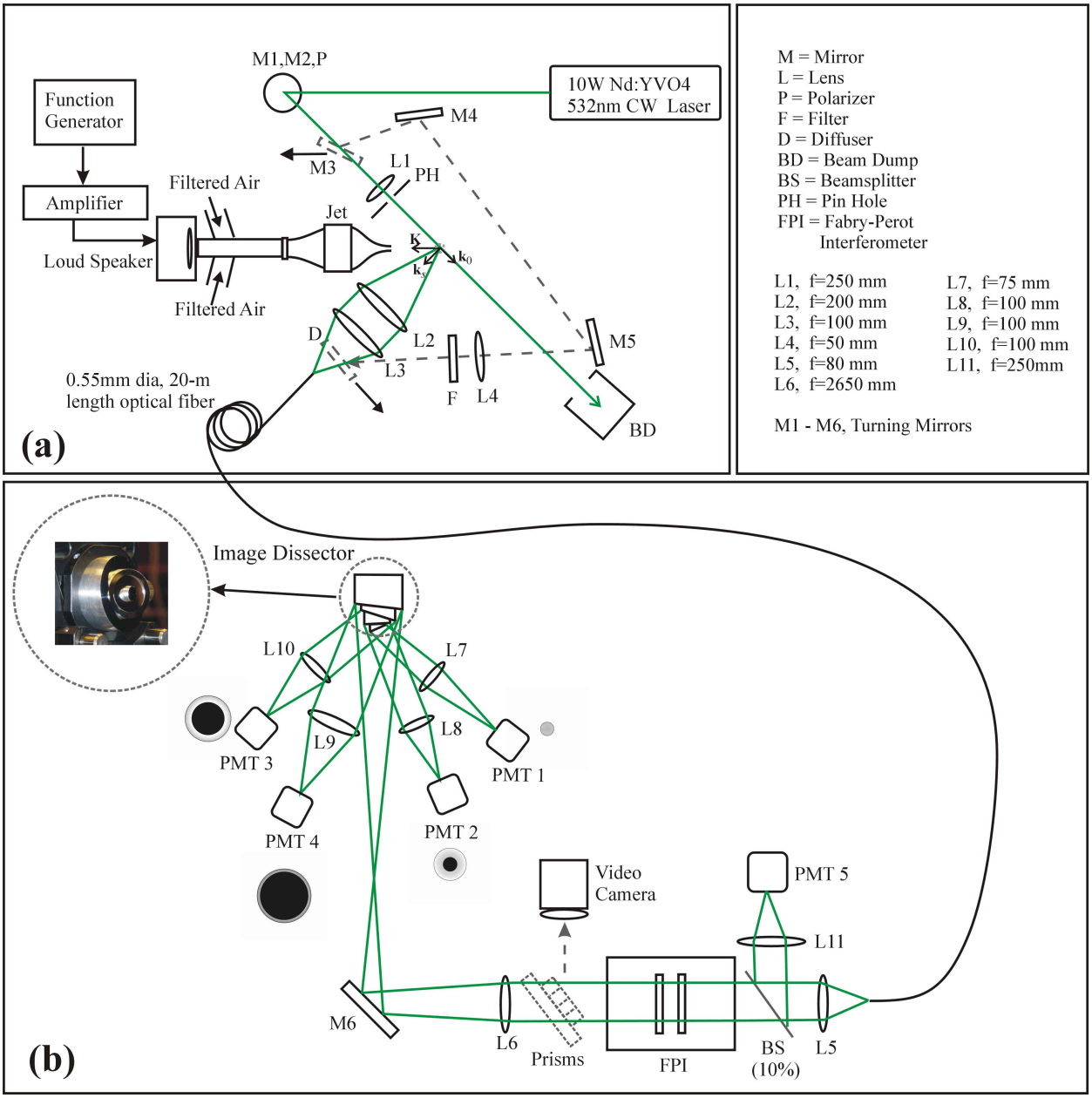

Figure 7. Diagram of experiment setup: (a) laser and collection optics; (b) spectral analysis and detection equipment.

The fiber was routed to a separate optical table where spectral analysis and detection took place, shown in Fig. 7b. The light exiting the fiber was collimated by an 80 mm focal length lens (L5) and was directed through the planar mirror FPI. The FPI had 70 mm diameter mirrors with 80% reflectivity, 8.7 GHz free spectral range (FSR), and reflective finesse of approximately 16. The Fabry-Perot is an extremely sensitive instrument; even the smallest vibrations or temperature changes can cause the mirrors to drift out of parallel alignment, resulting in increased uncertainty. Therefore, a stabilization system was utilized to maintain parallelism of the mirrors during testing. Between Rayleigh scattering measurements, a mirror and diffuser (Fig. 7a) were placed in the beam path by linear actuators to direct some of the incident laser beam into the optical fiber and through the FPI. A set of reflecting

prisms mounted on a linear actuator (Fig. 7b) was positioned in the optical path at the output of the interferometer to direct the light from three regions of the interferometer mirrors to a video camera. Live video of the three fringe images was used in a feedback control loop to adjust the mirror positions using piezoelectric transducers until the three fringes were equal in diameter. This system was also used to set the fringe diameter of the incident reference light to 13 mm, as determined from the uncertainty analysis. Further details regarding the mirror stabilization system for the FPI can be found in Ref. 17.

When flow measurements were collected the prisms, mirror, and diffuser were removed from the optical path and the light exiting the FPI was focused by a fringe forming lens (L6) having an effective focal length of 2650 mm, which provided an 18.2 mm diameter image of the fiber face. Light from circular and annular sections of the image were directed toward PMTs by a concentric elliptical mirror system, which was designed and fabricated specifically for this application. The 'image dissector' is shown in the upper left corner of Fig. 7b. The mirrors were machined from 6061 aluminum and the 12^o elliptical surfaces were diamond polished to a mirror finish. The mirror diameters, from innermost to outermost, are 5 mm, 12 mm, 16 mm, and 25 mm. Each mirror sends the respective portion of the fringe image toward PMTs 1, 2, 3, and 4, as labeled in Fig. 7b. The concentric mirror system is an improvement over the previous arrangement, which used a series of varying diameter 45^o elliptical mirrors and the fringe image had to be re-focused multiple times. The new image dissector eliminates the uncertainty involved in the re-imaging process. Figures 8 and 9 illustrate the individual areas of the fringe image which are directed towards each PMT.

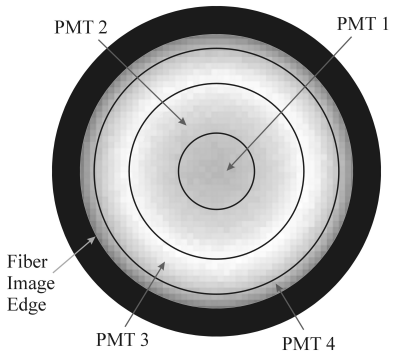

Figure 8. Dissection of Fabry-Perot fringe pattern into four annular regions.

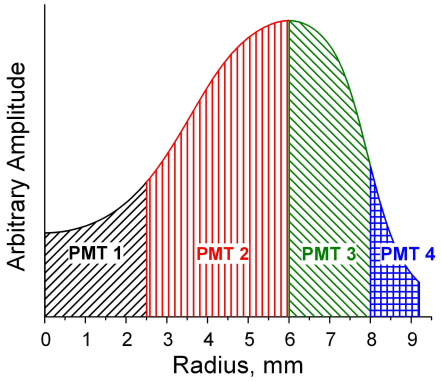

Figure 9. Radial slice of a fringe pattern showing the annular regions detected by the four PMTs. The amount of light in each region changes as the velocity and temperature fluctuate.

The PMTs were operated in the photon counting mode to acquire fringe intensity data. The photoelectron pulses from the five PMTs were amplified (Gain = 5) and sent to photon counters, which output NIM level pulses. Constant fraction discriminators converted the NIM pulses to 10 ns wide TTL level pulses that were counted via counter-timer boards. Typical photoelectron count rates for this work were on the order of 1 MHz. A PC-based data acquisition system was used to record the signals from the PMTs. Each signal channel was digitized at either 1 or 16 kHz sampling rate for 30 seconds, resulting in 30,000 or 480,000 samples per channel. The intensity information from the Fabry-Perot fringe sampling was used to obtain temperature and velocity measurements. The density measurement was much simpler, requiring only an overall intensity measurement. A beamsplitter located just in front of the FPI input (Fig. 7b) directed approximately 10% of the incoming Rayleigh scattered light to a lens (L11), which focused the light at PMT 5 for density measurement.

B. Electrically-heated low-speed jet

Flow measurements were performed downstream of a heated air stream issuing from an 8 mm diameter straight tube surrounded by a 50 mm diameter 2 m/s room temperature co-flow at the NASA Glenn Research Center using the described Rayleigh scattering measurement technique. A diagram of this system was presented in a previous publication[19]. The core flow was heated via electrically heated coils inside the tube, which generated turbulent mixing in the exiting air stream. The heated air jet was operated over a static temperature range of 295 to 700 K with a mean centerline velocity ranging from 8 to 12 m/s measured at an axial distance of 32 mm (4 jet diameters) from the tube exit. The Reynolds number ranged from 1500 - 3000. A PID feedback control unit was used to adjust and maintain the jet total temperature to within ± 1.5 K of the set-point temperature.

The temperature, density, and velocity measurements at the probe location were verified using additional instrumentation. A fine-wire (0.25 mm diameter) open-bead type K thermocouple provided jet static temperature data. A pressure gauge measured the ambient (static) pressure. Gas density information was derived using the ideal gas law. The jet velocity profile was evaluated from total pressure measurements with a pitot probe. A CCA (coldwire anemometry) system provided static temperature fluctuation measurements. The system consisted of a 1.3 μm diameter, 0.9 mm long platinum resistance wire operated in a constant current configuration. The frequency response of the CCA system, based on the 3 dB point, was measured to be approximately 1 kHz. Pitot probe and CCA measurements were obtained at the same jet conditions as the Rayleigh data, however they were not obtained simultaneously, and in some instances were not even acquired on the same day.

C. Acoustically-excited jet

The heated jet was replaced with a jet consisting of a converging nozzle with a 10 mm exit diameter. The jet was coupled to a loudspeaker, which provided pressure waves that induced velocity fluctuations of a known frequency in the exiting flow. A function generator provided a variable frequency sine wave input to the amplifier, which allowed variation of the signal amplitude sent to the speaker diaphragm. Measurements were performed at a location 2 jet diameters downstream of the nozzle exit. The jet was plumbed with filtered air, however due to the lack of a surrounding filtered co-flow, as in the heated jet system, measurements could only be made in the clean core flow of the jet stream to avoid scattering from particles entrained from the surrounding room air. The jet was operated over a plenum (total) pressure range of 100 – 127 kPa, which provided axial velocities in the jet core of 60 – 210 m/s (Mach 0.17 – 0.63) and temperatures of 297 – 277 K. The Reynolds number was on the order of 10^5. The loudspeaker was operated over a frequency range of 100 – 5000 Hz at a fixed amplitude.

For calibration purposes, the mean temperature, density, and velocity at the probe location in an un-excited flow were calculated via isentropic flow and ideal gas equations using total pressure and temperature measurements acquired by pressure probe and thermocouple measurements in the jet plenum. The velocity fluctuations were verified using a CTA (hotwire anemometry) system. The system consisted of a 3.8 μm diameter, 1.25 mm long platinum-coated tungsten resistance wire operated in a constant temperature configuration with an overheat ratio of 1.4. The frequency response of the CTA system was measured to be greater than 100 kHz. The CTA measurements were obtained at the same location and jet conditions as the Rayleigh data, but were acquired on a different day.

IV. Results

A. Calibration and technique verification

The technique was calibrated over the maximum range of operating points for each jet. The heated jet was capable of a static temperature range of 295 – 700 K and velocity range of 8 – 12 m/s. The unheated nozzle flow was operated over a static temperature range of 277 – 297 K and velocity range of 60 – 210 m/s. Thermocouple and pitot probe measurements were used to determine the mean temperature and velocity of the gas at the center of the heated jet plume 32 mm downstream of the tube exit for calibration of the technique. Since thermocouples measure the temperature of the metal probe bead rather than the gas temperature, there may be a difference between the actual gas temperature and the thermocouple measurement. These differences result from conduction losses down the thermocouple wire and radiation losses to the surroundings. The error in thermocouple-measured gas temperature was estimated to be less than ±3 K for the temperatures studied here. Gas density in the heated jet was derived from thermocouple and pressure probe measurements. Isentropic flow and ideal gas relations were used in conjunction with pressure probe and thermocouple measurements of the unheated jet plenum pressure and temperature to provide mean temperature, density, and velocity values in the jet core for calibration of the convergent nozzle flow system.

The photoelectron counts recorded by PMT 5 are linearly related to density as shown by the calibration curves in Fig. 10 for data acquired at two sampling rates (1 and 16 kHz) in both the hot and cold jet experiments. The photon counts of the 16 kHz sampling rate data sets are significantly lower than the 1 kHz data because the integration time of the instantaneous samples is 1/16 that of the 1 kHz data.

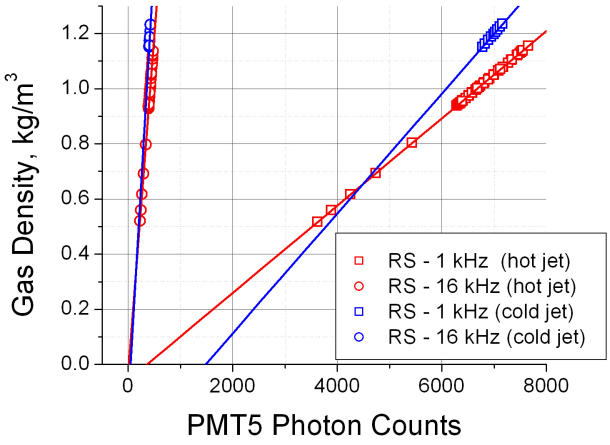

Figure 10. Density as a function of PMT 5 photon counts. (RS = Rayleigh Scattering)

The axial velocity component and temperature were measured simultaneously by analyzing the light from the circular and annular regions of the interference fringe pattern. A model of the fringe pattern, including the Rayleigh scattering spectrum and FPI instrument function, was used in a least squares fitting routine to estimate unknown parameters from the intensity data. Mean temperature, velocity, and pressure were either measured by physical probes or calculated from the isentropic flow relations and were used as known values in the least squares analysis of the mean photon count data at the calibration points, while several unknown factors were evaluated over the range of temperatures and velocities. These unknown factors included system detection efficiencies, effective finesse of the FPI, and fringe forming lens focal length. After these factors were calibrated and input in the model function, the mean PMT counts acquired at sampling rates of 1 and 16 kHz were analyzed to evaluate the mean temperature and velocity at each data point, with the constraint that the pressure was equal to the ambient pressure (which should be a valid assumption in these subsonic flows). Figures 11 and 12 respectively show mean temperature and velocity measurements from the Rayleigh technique compared with the isentropic values over the velocity and temperature calibration range in the unheated nozzle flow. The temperatures are accurate within a degree Kelvin and the velocities are within ± 5 m/s.

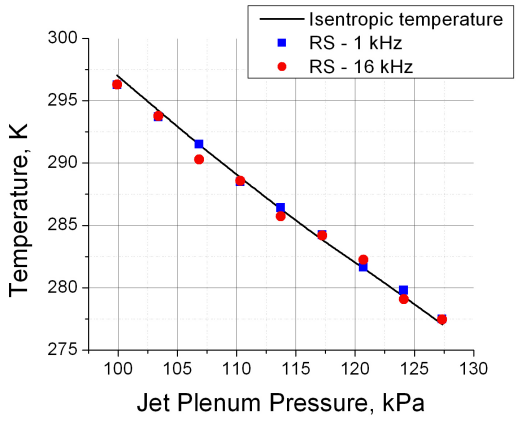

Figure 11. Mean temperature measurements from Rayleigh technique compared with isentropic values in the unheated nozzle flow.

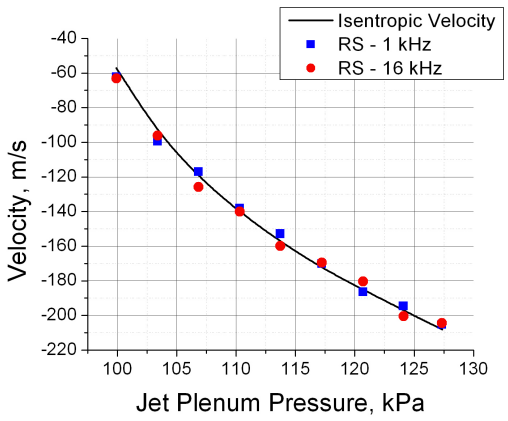

Figure 12. Mean velocity measurements from Rayleigh technique compared with isentropic values in the unheated nozzle flow.

In previous work, a significant bias error was observed in the mean velocity measurements[19]. After further investigation, it was found that this bias is mainly due to laser frequency drift (as much as 10 MHz drift over 30 seconds) and/or uncertainty in the reference fringe radius set point due to limitations of the Fabry-Perot stabilization

system. Attempts were made in the current work to eliminate some of the error by using fringe radius information recorded via the stabilization system software approximately 15 seconds prior to Rayleigh data acquisition and approximately 5 seconds after completion of the data acquisition. This allowed us to determine a more accurate reference fringe radius value for each measurement point, however it did not take into account radius change induced by laser frequency drift and/or Fabry-Perot mirror drift during the data acquisition time since we have no way of recording this information during collection of the Rayleigh signal. Using this radius information improved the velocity measurements slightly; however the bias is still on the order of 5 m/s.

Using the linear relation between PMT 5 photon counts and density (Fig. 10), and least squares analysis of the photon counts from PMTs 1-4, time histories of instantaneous density, temperature, and velocity were evaluated at each data point. The power spectra and mean square fluctuations were calculated from this information.

B. Power Spectral Density (PSD) calculations and temperature profiles in a heated jet

The Rayleigh probe volume and the CCA probe were scanned vertically across the centerline of the electrically-heated jet at an axial station of 32 mm. Scans were performed at centerline jet conditions of 360 K and 9 m/s. These radial scans provided measurements in the jet core as well as in the turbulent mixing layer formed between hot and cold air streams. Because of the shot noise in the PMT signals, it was necessary to use relatively long data records and calculate power spectral densities using a technique such as the Welch method of modified periodograms[26]. Due to extensive data processing time (approximately 700 samples/min), only the first 10 seconds of the 16 kHz data were analyzed. In the Welch method, a data record sampled at a rate f_s = 16 kHz (1 kHz) for a total time of 10 sec (30 sec) was subdivided into smaller records of length L = 2048 (128) samples, which were overlapped by 50%. The modified periodograms of each sub-record were calculated using a data window. These individual periodograms were then averaged to obtain the estimate of the power spectrum. The frequency resolution of the resulting spectra is f_s / L = 7.81 Hz. A sampling rate of 16 kHz was chosen so that the power spectra for both 1 and 16 kHz rates result in the same frequency resolution and the power levels in each frequency bin can be directly compared. Overlapping the segments by 50% provided a near maximum reduction in the variance in the spectral estimate. The resulting power spectral densities provide fluctuation information out to 8 kHz (0.5 kHz). The sum of all points in the PSD is equivalent to the mean square fluctuations.

Figure 13 shows temperature PSD plots for a measurement location in the shear layer (r_j = 5.5 mm) calculated from the 1 kHz CCA data and the 1 and 16 kHz Rayleigh data. This measurement location was chosen for demonstration of the technique since the highest amplitude temperature fluctuations occur in the shear layer. The 16 kHz PSDs have only been shown out to 2 kHz since the spectrum is flat and uninteresting beyond this point. The Rayleigh data records were processed using two different thermodynamic assumptions: a) constant static pressure (isobaric assumption); b) instantaneous pressure calculated from density measured via PMT 5 and temperature evaluated in the least-squares fit (non-isobaric assumption). The assumption used for each data set is indicated in the legend of Fig. 13. An isobaric assumption is typically valid in the subsonic flows studied here, however non-isobaric analysis is presented to show the applicability of this technique in situations where the pressure is unknown and possibly not constant, as in supersonic flows with shock waves. The non-isobaric assumption leads to significantly greater noise levels in the resulting measurements, as demonstrated by the magenta and grey colored curves in Fig. 13. The noise in the results is primarily due to shot noise.

Two numerical processing methods exist that are commonly used to eliminate noise from the power spectrum. Shot noise is broadband noise that contributes equally over all frequencies; therefore it causes a constant offset or noise floor in the spectrum. If the spectrum flattens out, as the 16 kHz spectrum does at higher frequencies where there are no significant temperature fluctuations, then the average value of this noise floor can be subtracted from every point in the spectrum, eliminating the broadband shot noise contribution. This procedure was used to eliminate shot noise in the 16 kHz Rayleigh data. The second method, which is only possible if you have two simultaneous measurements of the same property, is to take the cross-spectrum[27] of the two simultaneous, independent measurements. Any uncorrelated noise will be eliminated from the final spectrum. One way to obtain the two simultaneous measurements is to split the light into two separate paths and individually analyze each beam path. This would require a secondary set of all spectral analysis and detection equipment, which is not really practical. However, in our experiment the fringe image is resolved into four regions (concentric rings) from which we fit for only two unknown parameters. Theoretically, we can fit for four total unknowns, or fit two of the regions for the two unknowns (T and u_k) and fit the other two regions for the same two unknowns. The latter is the approach we took in order to obtain two simultaneous measurements of temperature and velocity. The cross-spectrum of the 1 kHz data processed in this manner is shown in Fig. 13. The cross-spectrum (green curve) matches more closely with the CCA measurements than the individual power spectrum (magenta curve) using the non-isobaric assumption. The cross-

spectrum processing method makes this technique useful even in situations where the measurements contain high noise levels, as in the case where the pressure may be unknown.

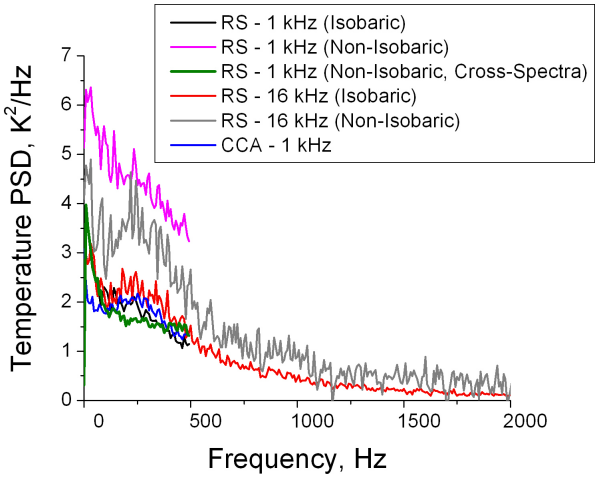

Figure 13. Power spectral density of temperature fluctuations in jet shear layer.

The mean temperatures were calculated from the time history data, and the turbulence temperature fluctuations were derived from the power spectral density calculations by taking the sum of all points in the PSD. Figures 14 and 15 show profiles resulting from radial scans across the jet flow of the mean temperature and turbulent temperature fluctuations calculated from the 1 kHz CCA measurements and the 1 and 16 kHz Rayleigh measurements, processed as described above using the noted thermodynamic assumptions. The mean temperature values have some scatter between the various data sets; however, the greatest deviation is still less than 3% error. The CCA measurements provide very accurate turbulence levels for fluctuations up to 0.5 kHz; however, as the 16 kHz power spectra show (Fig. 13), significant temperature fluctuations still exist beyond 0.5 kHz. Since the 1 kHz CCA and Rayleigh measurements do not account for higher frequency fluctuations, the resulting turbulence levels from these data sets may be lower than the true temperature fluctuations over all frequencies. Based on the rule of thumb that the peak shear layer fluctuations are approximately 15-18% of the difference between the centerline and ambient temperatures, the peak fluctuations are expected to be on the order of 10-12 K. All of the data sets, especially those where noise removal methods were employed, provide fluctuations that exhibit the typical profile shape and are near to the expected magnitude for these measurements.

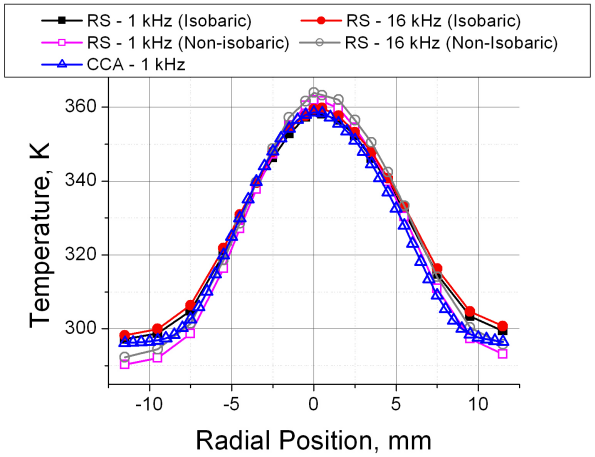

Figure 14. Mean temperature profile at an axial station 32 mm downstream of the tube exit.

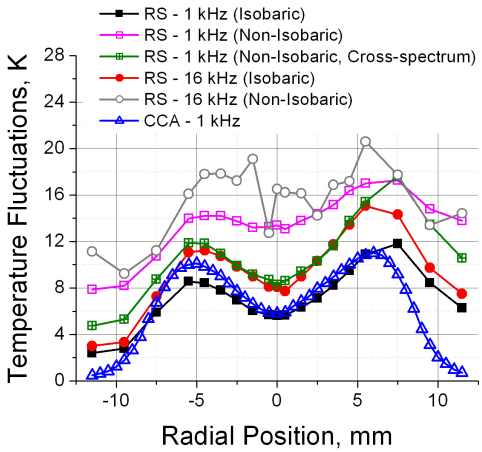

Figure 15. Temperature fluctuation profiles at an axial station 32 mm downstream of the tube exit.

C. PSD calculations in an acoustically-excited jet

The unheated nozzle flow was operated at a mean velocity of 60 m/s while the flow velocity was perturbed by acoustically-induced pressure waves emanating from a loudspeaker at frequencies from 100 Hz up to 5000 Hz. The frequencies were set approximately to the desired values by a knob on the function generator. The exact excitation frequencies were not measured and may be slightly different than the noted values. Flow measurements were made using the Rayleigh technique and hotwire anemometry (CTA). Both instrumentation systems were sampled at 1 and 16 kHz. The Rayleigh data was processed using the isobaric assumption along with the two-ring simultaneous fit method described in the previous section, and cross-spectral calculations were used to eliminate noise in the measurements. The hotwire measurements showed that the induced velocity fluctuation amplitude was approximately 3 m/s, in most cases. However, the 3000 Hz excitation frequency produced fluctuations of 6 m/s. Further investigation into the flow dynamics is necessary to understand the reason for the higher fluctuations at this excitation frequency. Figure 16 shows velocity PSDs calculated from Rayleigh and hotwire data acquired at 1 kHz for acoustic excitations up to 400 Hz. Peaks in the spectra are observed at the expected frequencies in both Rayleigh and hotwire data, although the amplitude of the Rayleigh peaks is typically about ½ that of the hotwire peaks. The velocity fluctuations are actually quite low due to inefficient coupling of the acoustic waves to the jet flow. If the velocity fluctuations were higher in amplitude the measurement error would probably be significantly reduced. The 400 Hz peak for the Rayleigh data is extremely strong, having an amplitude of 95 $(m/s)^2/Hz$ (the plotting range was limited so that the lower amplitude peaks can be seen). However, the hotwire data indicates the peak amplitude is 2.3 $(m/s)^2/Hz$, showing that the fluctuations are not really that great at this frequency. It is speculated that the 400 Hz frequency is coupling with the 430 Hz resonant frequency typically observed in the laser system[19] causing artificially high power in the spectrum at that excitation frequency.

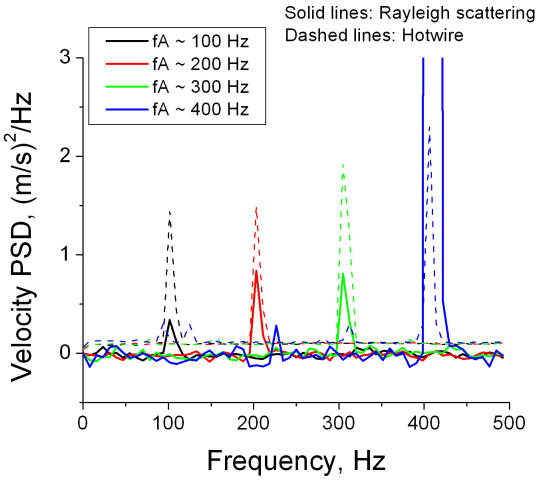

Figure 16. Power spectral density plots of Rayleigh and hotwire data acquired at 1 kHz in the acoustically excited jet.

Figures 17 and 18 show velocity PSDs calculated from Rayleigh and hotwire data acquired at 16 kHz for acoustic excitations up to 5000 Hz. Peaks in the spectra are observed at the expected frequencies in both Rayleigh and hotwire data. At some frequencies the Rayleigh peaks are greater in amplitude than the hotwire peaks, while in other cases it is the opposite situation. The laser system may be sensitive to certain frequencies, causing induced resonance in the laser frequency resulting in artificially large velocity fluctuations at those excitation frequencies. Further investigation into the discrepancies will be done in future work, as well as improving the acoustic coupling to provide higher amplitude velocity perturbations. This initial investigation of an acoustically-excited jet presents the first attempt at validating velocity fluctuation and frequency prediction of the Rayleigh scattering technique using an externally forced flow.

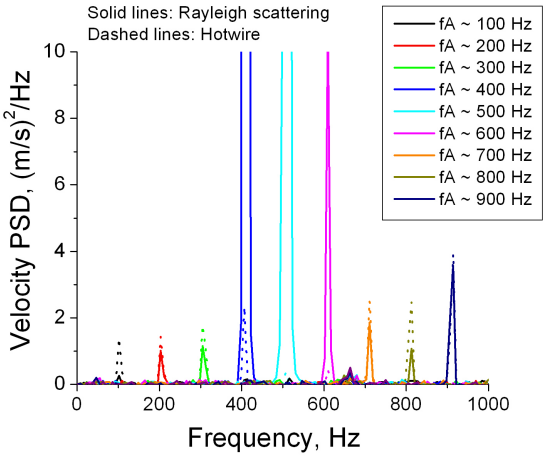

Figure 17. Power spectral density plots of Rayleigh and hotwire data acquired at 16 kHz in the acoustically-excited jet (lower end of excitation frequency range).

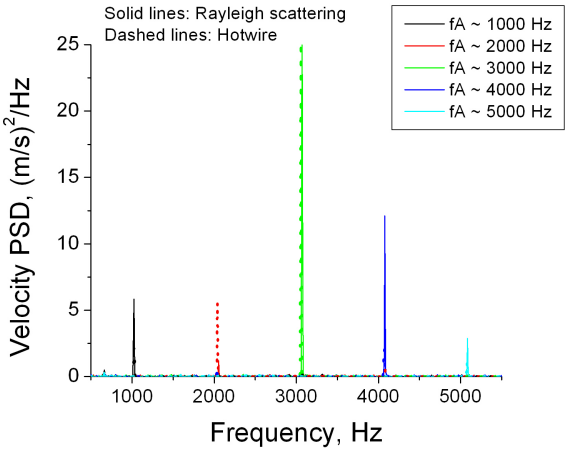

Figure 18. Power spectral density plots of Rayleigh and hotwire data acquired at 16 kHz in the acoustically-excited jet (higher end of excitation frequency range).

V. Conclusion

A technique for obtaining dynamic gas temperature, velocity, and density measurements using molecular Rayleigh scattering was described. Density was determined from an overall intensity measurement of the scattered light, while temperature and velocity were determined by analyzing the scattered light with a Fabry-Perot interferometer. The signals from five photomultiplier tubes were simultaneously recorded using photon counting electronics operating at 1 and 16 kHz sampling rates with 30 and 10 second recording periods. An uncertainty analysis was presented that demonstrated uncertainties in instantaneous temperature, velocity, and density measurements of about 6%, 12 m/s, and 3.5%, respectively, for a 16 kHz sampling rate. Derived statistical quantities, such as mean square fluctuations and power spectra, can be obtained with high accuracy, especially when inherent noise contributions are eliminated. The noise in the measurements was minimized numerically in the data processing either by subtracting the broadband shot noise contribution, or taking the cross-spectrum of two simultaneous, independent measurements. Measurements using the Rayleigh technique were demonstrated in a low speed heated air flow where temperature fluctuations were verified with CCA measurements, and in an acoustically-excited nozzle flow where velocity fluctuation and frequency were verified with CTA measurements.

In future work, we hope to further improve the velocity measurements by resolving the issues related to the bias error (i.e., laser frequency instability and uncertainty in the reference fringe radius). We would like to perform a similar acoustic-excitation test to verify the temperature fluctuation and frequency measurement. A system of acoustically-excited opposed jets in which one is electrically heated and one is unheated will allow such measurements. The efficiency of the data processing methods will also be improved to speed up the analysis time. The presented Rayleigh scattering technique will eventually be used in aeroacoustics research, where sound pressure fluctuation (microphone) measurements will be acquired simultaneously with Rayleigh measurements allowing correlation between flow property fluctuations and noise generation. Determining sources of jet noise will help engineers to design quieter, more efficient aircraft.

Acknowledgments

We would like to thank Dick Seasholtz for his technical advice, and Kairul Zaman and Robert Boyle for supplying the hotwire equipment and providing their valuable expertise in hotwire anemometry.

References

[1]Eckbreth, A. C., *Laser Diagnostics for Combustion Temperature and Species*, Gordon and Breach Science Publishers SA, Amsterdam, 1996, pp.209-451.

[2]Cummings, E. B., "Laser-Induced Thermal Acoustics," Ph.D. Dissertation, Department of Engineering and Applied Science, California Institute of Technology, Pasadena, CA, 1995.

[3]Hart, R. C., Balla, R. J., and Herring, G. C., "Nonresonant referenced laser-induced acoustics thermometry in air," *Appl Optics*, Vol. 38, No. 3, 1999, pp. 577-584.
[4]Li, Y., Roberts, W. L., and Brown, M. S., "Investigation of gaseous acoustic damping rates by Transient Grating Spectroscopy," *AIAA Journal*, Vol. 40, No. 6, 2002, pp. 1071-1077.
[5]Lau, J. C., Morris, P. J., and Fisher, M. J., "Measurements in subsonic and supersonic free jets using a laser velocimeter," *J Fluid Mech*, Vol. 93, Jul, 1979, pp. 1-27.
[6]Lau, J. C., Whiffen, M. C., Fisher, M. J., and Smith, D. M., "A note on turbulence measurements with a laser velocimeter," *J Fluid Mech*, Vol. 102, Jan, 1981, pp. 353-366.
[7]Flack, R. D., "Influence of turbulence scale and structure on individual realization laser velocimeter biases," *J Phys E: Sci Instrum*, Vol. 15, No. 10, 1982, pp. 1038-1044.
[8]Heist, D. K., Castro, I. P., "Point measurement of turbulence quantities in separated flows-a comparison of techniques," *Meas Sci Technol*, Vol. 7, No. 10, 1996, pp. 1444-1450.
[9]Elliott, G. S., and Boguszki, M., "Filtered Rayleigh scattering: toward multiple property measurements," AIAA-2001-0301, 2001.
[10]Bridges, J., Wernet, M. P., and Brown, C., "Control of jet noise through mixing enhancement," NASA TM-212335, 2003.
[11]Garg, S., and Settles, G. S., "Measurements of a supersonic turbulent boundary layer by focusing schlieren deflectometry,"*Exp Fluids*, Vol. 25, No. 3, 1998, pp. 254-264.
[12]Seasholtz, R. G., and Greer, L. C., "Rayleigh scattering diagnostic for measurement of temperature and velocity in harsh environments," AIAA-98-0206, 1998.
[13]Panda, J., and Seasholtz, R. G., "Velocity and temperature measurement in supersonic free jets using spectrally resolved Rayleigh scattering," AIAA-99-0296, 1999.
[14]Mielke, A. F., Seasholtz, R. G., Elam, K. A., and Panda, J., "Time-average measurement of velocity, density, temperature, and turbulence velocity fluctuations using Rayleigh and Mie scattering," *Exp Fluids*, Vol. 39, No. 2, 2005, 441-454.
[15]Lock, J. A., Seasholtz, R. G., and John, W. T., "Rayleigh-Brillouin scattering to determine one-dimensional temperature and number density profiles of a gas flow field," *Appl Optics*, Vol. 31, No. 15, 1992, pp. 2839-2848.
[16]Seasholtz, R. G., and Panda, J., "Rayleigh scattering diagnostic for dynamic measurement of velocity and temperature," AIAA-99-0641, 1999.
[17]Seasholtz, R. G., Panda, J., and Elam, K. A., "Rayleigh scattering diagnostic for measurement of velocity and density fluctuation spectra," AIAA-2002-0827, 2002.
[18]Mielke, A. F., and Elam, K. A., "Molecular Rayleigh scattering diagnostic for measurement of high frequency temperature fluctuations," *Proceedings of SPIE Optical Diagnostics Conference*, Vol. 5880, The International Society of Optical Engineering, Bellingham, WA, 2005, pp. K1-K12.
[19]Mielke, A. F., Elam, K. A., and Sung, C. J., "Rayleigh scattering diagnostic for measurement of temperature, velocity, and density fluctuation spectra," AIAA-2006-837, 2006.
[20]Tenti, G., Boley, C., D., and Desai, R. C., "Velocity and temperature measurement in supersonic free jets using spectrally resolved Rayleigh scattering," *Can J Phys*, Vol. 52, No. 4, 1974, pp. 285-290.
[21]Sandoval, R. P., and Armstrong, R. L., "Rayleigh-Brillouin spectra in molecular nitrogen," *Phys Rev A*, Vol. 13, No. 2, 1976, pp. 752-757.
[22]Yip, S., and Nelkin, M., "Application of a kinetic model to time-dependent density correlations in fluids," *Phys Rev*, Vol. 135, No. 5A, 1964, pp. A1241-A1247.
[23]Boley, C. D., Desai, R. C., and Tenti, G., "Kinetic models and Brillouin scattering in a molecular gas," *Can J Phys*, Vol. 50, No. 18, 1972, pp. 2158-2173.
[24]Vaughan, J. M., *The Fabry Perot Interferometer, History, Theory, Practice, and Applications*, Adam Hilger, Philadelphia, 1989, pp. 89-134.
[25]Whalen, A. D., *Detection of Signals in Noise*, Academic Press, New York, 1971, pp. 327-332.
[26]Welch, P. D., "The use of fast Fourier transform for the estimation of power spectra: A method based on time averaging over short, modified periodograms," *IEEE Trans on Audio and Electroacoustics*, Vol. AU-15, No. 2, 1967, pp. 70-73.
[27]Oppenheim, A. V., and Schafer, R. W., *Digital Signal Processing*, Prentice-Hall, New Jersey, 1975, pp. 554-555.